


Research Article

# Downstream Morphological and Sedimentary Transformations in Modern Continental-Scale Rivers

Abdullah M. Wahbi<sup>1,2</sup>, Michael D. Blum<sup>1</sup> 

<sup>1</sup> Earth, Energy and Environment Center, University of Kansas, <sup>2</sup> Saudi Aramco (Saudi Arabia)

Keywords: Normal-Backwater Transitions, Sedimentary Reconstructions, Scaling Relationships

<https://doi.org/10.2110/001c.90009>

---

## The Sedimentary Record

Vol. 21, Issue 1, 2023

---

Morphological characteristics in river systems, including channel dimensions and river gradients, scale to drainage basin area, which provides the means for such elements to be predicted, measured and modeled. Moreover, recent studies interpret downstream changes in channel morphological and sedimentary characteristics to be the product of changing flow hydraulics as rivers transit from the normal flow to the backwater reach and approach the coastal ocean. This paper quantifies how large modern rivers undergo morphological and sedimentary transformations in response to normal flow to backwater transition.

Morphologies adapting to such backwater hydraulic conditions is a potential for further investigation. With applications in modeling of modern river systems, this also provides the means for paleoenvironment reconstructions based on changing morphological characteristics since such quantitative framework is grounded by similar depositional processes.

Building on previous studies, we construct river-long profiles, estimate backwater lengths, measure the ratio between channel-belt and channel widths ( $B_{ChB}/B_{Ch}$ ), and measure the ratio between sand-rich to mud-dominated environments of deposition (S/M ratio) in five large modern river systems. We use results from >55,000 measurements of morphological and lithological characteristics from ~3,850 valley cross-sections over ~5,500 river kilometers to show that: (a) channel gradients decrease by ~30-50% as the channel goes through the normal flow to backwater transition, whereas (b)  $B_{ChB}/B_{Ch}$  decreases by >~60% and (c) S/M ratios decrease by ~35-90% within the upper backwater reach. These values further decrease in the lower backwater reach and approach unity ( $B_{ChB}/B_{Ch} = 1$ ; S/M = 0) as the gradient reaches zero (sea level). Such systematic transformations in morphologic and sedimentary characteristics indicate they are both inherent and predictable, and can be used to interpret normal flow vs. backwater hydraulics in ancient fluvial deposits.

## INTRODUCTION

Development and application of the source to sink (S2S) approach (e.g., Romans et al., 2016) is fundamentally based on the uniformity of process over time. For modern systems, it is possible to observe, quantify and model processes and rates, characteristics of source terrains, the sediment-routing systems, and sediment sinks. Indeed, from several decades of studying modern systems, it is clear that many fluvial system variables scale directly or inversely to contributing drainage area: these include channel sizes and shapes, river and shelf gradients, sediment loads, and the dimensions of basin-floor fans (Blum et al., 2013; Fernandes et al., 2016; Milliken et al., 2018; Nyberg, Gawthorpe, et al., 2018; Nyberg, Helland-Hansen, et al., 2018; Sømme et al., 2009; Syvitski & Milliman, 2007 and others).

The morphology of modern river channels within continental interiors is well known to reflect adjustments of channel size, shape, and gradient so as to transport water volumes and the sediment grain size and volume provided from the contributing drainage area (e.g., Brice, 1974; Carey, 1969; Church, 2006; Dade, 2000; Dade & Friend, 1998; Hickin, 1974; Hickin & Nanson, 1975; Jackson, 1976; Knighton, 1992; Langbein, 1964; Langbein & Leopold, 1970; Leopold & Langbein, 1966; Leopold & Maddock, 1953; Leopold & Wolman, 1960; Lewin, 1983; Schumm, 1977). Moreover, recent first-generation studies also describe characteristic downstream transformations in channel morphology and depositional processes as river channels go through the transition from normal flow to backwater hydraulic conditions where they are influenced by the presence of the ocean (Blum et al., 2013; Fernandes et al., 2016; Hartley et al., 2017; Li et al., 2006; Martin et al., 2018; Milliken et al., 2018; Nittrouer et al., 2011;

Passalacqua et al., 2013; Wilson & Goodbred, 2015). For example, rivers entering their backwater reach experience downstream reductions in water-surface slopes and bed-load sediment transport rates during low flow, increased rates of deposition, and downstream decreases in channel migration rates and associated channel-belt widths: these transformations, in turn, favor channel avulsion over lateral migration (e.g., Blum et al., 2013, 2017; Fernandes et al., 2016; Hudson & Kesel, 2000; Leuven et al., 2018; Martin et al., 2018; Milliken et al., 2018; Paola & Martin, 2012; Prasojo et al., 2022; Prokocki, 2017; Sandbach et al., 2018; Sincavage et al., 2019; Strong et al., 2005; Syvitski et al., 2022). Such phenomena have been described in previous studies, but a more quantitative understanding of how scaling relationships change through the transition from normal flow to backwater hydraulic conditions remains to be demonstrated.

In addition to applications in geomorphology, hydrology or ecology, S2S concepts that are grounded in scaling relationships can also be inverted to reconstruct ancient sediment-routing systems and provide insight into ancient tectonic settings (e.g., Allen, 2008; Densmore et al., 2007; b; see especially Martin et al., 2018). One example where such applications can have an impact is the Lower Cretaceous McMurray Formation (see Wahbi et al., 2022), where seemingly irreconcilable environments of deposition have been interpreted over the last few decades: one interpretation places McMurray deposits within an estuary and near the shoreline under the influence of tidal processes and brackish water, whereas an alternative model favors a fully fluvial environment of deposition that is unaffected by marine processes (Blum, 2017; Gingras & Leckie, 2017; Moreton & Carter, 2015; Peng et al., 2022; Shchepetkina et al., 2016, 2019). The McMurray example represents a case where interpretation of depositional environment would significantly benefit from additional criteria for recognition and interpretation of environments.

In this paper, we seek to further understand downstream morphological and sedimentary transformations in large modern rivers as a function of changing hydraulic conditions within the backwater reach, and we seek to do so within a framework that can be used to understand modern rivers, and interpret ancient strata as well.

## DOWNSTREAM TRANSFORMATIONS THROUGH THE NORMAL FLOW TO BACKWATER TRANSITION

Previous studies show that the upstream distance over which backwater hydraulic conditions occur scales as  $L_B = H_{Ch}/S$ , where  $L_B$  = backwater length (km),  $H_{Ch}$  = channel depth (m), and  $S$  = slope (m/m) (Paola & Mohrig, 1996).  $L_B$  therefore scales to the size of the river system, and, in a practical sense, to the location where the mean depth of the channel descends below sea level:  $L_B$  can be <10s of kms for steep and shallow gravel-bed rivers, but it can also be hundreds of kilometers long in low-gradient sand-bed rivers with deep channels (Blum et al., 2013). As a result, there can be hundreds of kilometers within the backwater reach of large rivers that are downstream from the normal flow

reach, but experience tidally modulated flow (Gugliotta & Saito, 2019).  $L_B$  generally scales to the distance over which channel slope and hydraulic energy decreases (e.g. Syvitski et al., 2022), marine-attached avulsions become common, and a distributary channel system develops (e.g., Chamberlain & Hajek, 2019; Ganti et al., 2014; Jerolmack & Swenson, 2007; Prasojo et al., 2022), which results in construction of delta plains. However, while a significant part of the backwater reach can be impacted by tidal currents, the backwater reach and tidal river are not synonymous with the distance over which saltwater can penetrate upstream into the river channel. Instead, the channels of large rivers are typically characterized by the inland migration of bottom-hugging salt-water wedges during periods of seasonal low flow that are significantly less thick than the channel as a whole (e.g., Carlin et al., 2015; Galler & Allison, 2008; Geyer & MacCready, 2014; Harleman, 1991; Ibañez et al., 1997; Kineke & Sternberg, 1995), whereas seasonal average to high flow push saltwater completely out of the river channel into the coastal ocean.

We selected five large modern river systems for comparative study: these are the Mississippi River in the United States, the Paraná River in Argentina and Paraguay, the Niger River in Nigeria, the Indus River in Pakistan, and the Irrawaddy River in Myanmar. Although we do no analyses on the Amazon River, we include long profiles and other information for the Amazon River as an end-member. The selected rivers are among Earth's 30 largest modern river systems (e.g., Milliman & Farnsworth, 2013; Syvitski & Milliman, 2007), but differ in scale, discharge, sediment load, and the degree of tidal influence and saltwater penetration in deltaic regions. These river systems were selected from different continents and latitudes to test if they show similar downstream morphological and sedimentary transformations. For each system, we measure morphological and sedimentary parameters from satellite images that are readily accessible in Google Earth, which also includes multiple satellite elevation datasets for different parts of the world with spatial resolutions of 30 m, and vertical resolutions of  $\pm 30$  m. We address three sets of parameters (Figure 1), as follows:

1. Starting at the river mouth we construct generalized longitudinal profiles along each river by tracing the lower ~800 – 1500 river kilometers (hereafter RK) for each channel in Google Earth, then extract the channel elevation every 25 RK, and calculate the long profile as a 2<sup>nd</sup> order polynomial fit. We then identify the likely transition from normal flow to backwater hydraulics based on downstream decreases in channel slope, as well as the downstream narrowing of the low-flow channel and decreased exposure of unvegetated channel bars, and use these observations to identify a 50 RK reach along each river that we interpret to include  $L_B$ , and the normal flow to backwater transition.
2. We compile data from the literature on the inland penetration of tidal signals and saltwater for each river system to illustrate scaling relationships between these variables and the backwater reach. Al-

though we note the inland penetration of tides and saltwater in the Indus River from the published literature, present-day conditions are strongly related to the anthropogenically induced modification of the channel and channel migration rates, which are a result of large reductions in discharge and sediment loads due to dam construction (see Syvitski et al., 2014).

3. For each river, we measure active channel widths ( $B_{Ch}$ ) and channel-belt widths ( $B_{ChB}$ ) from valley cross-sections oriented perpendicular to the channel belt and located every ~1-3 RK. We define a channel belt as the area in which multiple channel sandbodies were deposited as a result of channel migration within one avulsion cycle (Jobe et al., 2020; Nyberg et al., 2023). Our measured cross-sections begin near the river mouth for each river and continue upstream hundreds of river kilometers into the normal flow reach. When measuring  $B_{Ch}$ , special attention was paid to capturing bankfull width in a consistent manner, since satellite images can change from one location to another in a single river system. For  $B_{ChB}$ , we measure the width of laterally amalgamated scroll topography to quantify how far the channel migrated to produce the dominantly sand-rich environments of deposition (utilizing the time-span feature in Google Earth to constrain the historical extent of channel migration within the channel belt). We then calculate the dimensionless ratio  $B_{ChB}/B_{Ch}$  as a normalized measure of the distance over which the channel has migrated during channel belt construction.
4. Last, for each river system we measure the percentage of each cross-section that is dominated by sandy vs. muddy environments of deposition, by recording observable characteristics every 500 m along each cross-section. We classify the environment as sand-dominated based on the presence of arcuate scroll topography that forms from lateral accretion as the channel migrates laterally, and classify the environment as mud-dominated flood plain in the absence of scroll topography and the presence of features like distributary channels, crevasse channels and crevasse splays. Recognition of active vs. abandoned channel segments is straightforward: although most modern abandoned channels still contain standing water, we classify them as mud-filled because we assume they will not receive significant new sand input from the active river channel, and they will be preserved in the stratigraphic record as a mud-dominated environment of deposition. From these data, we calculate the distribution of sandy vs. muddy environments of deposition for each cross-section as the sand-to-mud ratio (hereafter S/M ratio).

## RESULTS

We measured channel gradients over a sum total of ~5,500 RK in the five large modern rivers we focus on to estimate the normal flow to backwater transition (see Table SM1 in Supplementary Material). Our measurements of

$B_{ChB}/B_{Ch}$  ratios, and S/M ratios come from 3,853 cross-valley transects in the five primary rivers of our study, with transects oriented perpendicular to channel-belt trends (and equivalent to channel-belt widths) at an average spacing of ~1.4 RK. A total of 7,597 channel width measurements were made across these transect lines: if more than one channel was identified in the transect, we calculate channel width as the sum of the 3 widest channels. A total of 43,575 measurements of sandy vs. muddy environments of deposition were similarly recorded for all transect lines (Tables SM2-SM6). In general, these data were collected over channel lengths that represent the backwater reach, and extend upstream into the normal flow reach over length scales that we estimate to be  $\geq 2L_B$  for each river system. For perspective, although these are some of the largest river systems on Earth, our measurements represent only the lower ~20-70% of the total river channel lengths (Linke et al., 2019) for the five river systems (see Figure 2; Table SM7).

We estimate  $L_B$  from downstream changes in channel gradient and the last downstream appearance of widespread emergent channel bars at low flow.  $L_B$  scales to contributing drainage area (Figure 2), which reflects the well-known inverse relationship between drainage area and channel gradient (e.g. Flint, 1974): we estimate  $L_B$  to be ~600 RK for the Mississippi River, the largest of the 5 rivers we examined, and between ~300-400 RK for the others. Channel gradients are generally very low, with downstream trends within the normal flow and backwater reaches that are consistent across the 5 river systems, and with results from previous studies (e.g., Blum et al., 2013; Fernandes et al., 2016). Gradients in the normal flow reach are generally  $<0.0001$  ( $1 \times 10^{-4}$ ) for all five river systems, but gradients in the normal flow reaches of each river are on average ~2.3 times the gradients in the upper backwater reach, and ~3.4 times steeper than channel gradients in the lower backwater reaches for the same rivers. Gradients in the lower backwater reach range from 0.00005 ( $5 \times 10^{-5}$ ) for the Niger River to 0.00002 ( $2 \times 10^{-5}$ ) for the Irrawaddy and Paraná Rivers (Figure 2; Table SM8). These observed downstream reductions in channel gradient are consistent with what has been referred to as the break between fluvial and deltaic environments, and downstream reductions in hydraulic energy that, on a global scale, has been estimated to average ~76% (Syvitski et al., 2022).

We have also compiled data on the upstream penetration of tidal signals and saltwater penetration in river channels from a variety of sources (e.g. Abam & Fubara, 2022; Abam & Omuso, 2000; Eisma, 1998; Giosan et al., 2006; Hedley et al., 2010; Kravtsova et al., 2008; Matsoukis et al., 2023; Obowu & Abam, 2014; Parsa & Shahidi, 2010; Sakai et al., 2021; Soileau et al., 1990; Syvitski et al., 2014; Taft & Evers, 2016; Velden, 2015; Wang et al., 2019). The presence of tidal signals defines the tidal river for each system, and in the 5 systems we studied, the tidal river and the estimated backwater length are essentially the same only in the macrotidal Irrawaddy River (~300 RK). By contrast, the microtidal Mississippi River records tidal signals up to ~375 RK upstream, which corresponds to the upper to lower



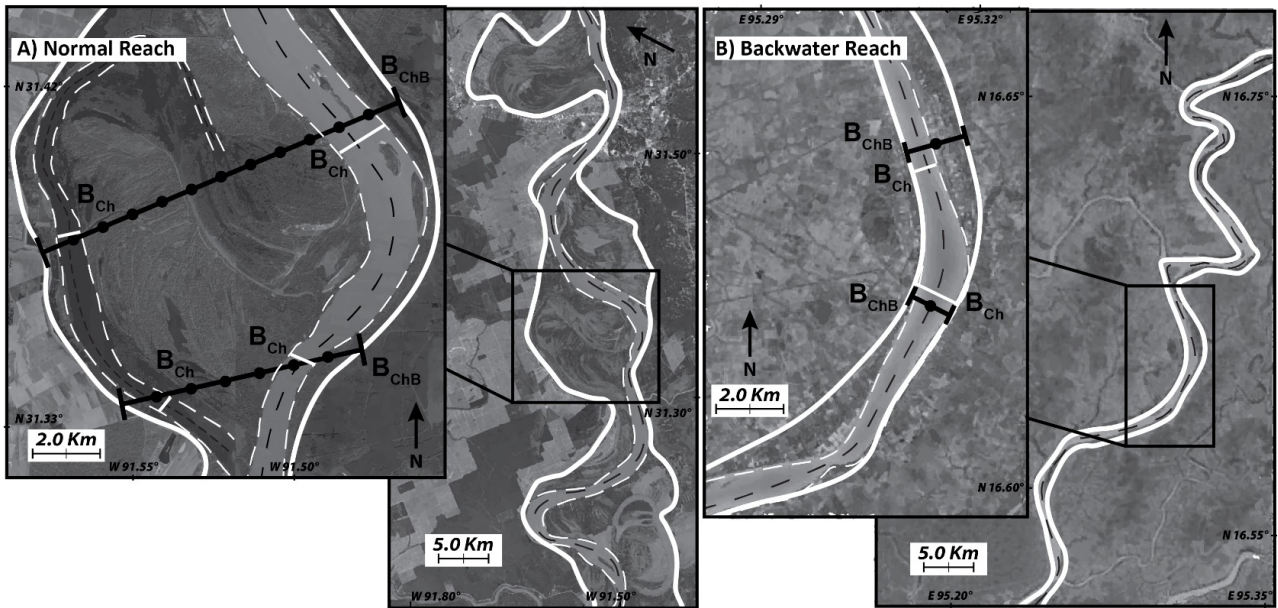


**Figure 1.** Examples of the current modern river measurements from: A) the Mississippi River normal reach, and B) the Irrawaddy River backwater reach. We first constrain the main active river channel (black dashed lines; including subordinate channels that receive water during river flood events) to measure river distance. We constrain channel belt boundaries (thick white lines), and channel widths (transect white lines). Channel belt transect lines (black) are used to estimate  $B_{ChB}/B_{Ch}$  ratios, such that  $B_{ChB}$  is the total transect length, and  $B_{Ch}$  is the total channel widths (if multiple channels exist). S/M ratios are estimated by taking a lithology measurement (sand-dominated vs. mud-dominated) every 500 m across transect lines based on apparent lithology (filled black circles along transect lines). Images modified from Google Earth.

backwater transition, whereas for the micro-tidal Paraná, and the mesotidal Niger and Indus rivers, tidal signals extend into the upper backwater reach, penetrating ~220 RK, ~175 RK, and ~160 RK, respectively (Figure 3; Table SM9).

Saltwater penetrates into river channels during seasonal low flow as a bottom-hugging saltwater wedge that will eventually mix and rise to the surface in dilute form then be flushed to the coastal ocean when discharge increases (e.g., Geyer & MacCready, 2014). In the 5 systems we examine, saltwater wedges penetrate into channels over distances that range from 0–160 RK (Figure 3; Table SM9). On one end of the spectrum, the Paraná River has significant freshwater discharge during all seasons, such that saltwater does not penetrate from the Rio de la Plata estuary into the channel at all. By contrast, saltwater wedges do penetrate upstream in large rivers with seasonal periods of low flow, but will then be pushed out into the coastal ocean during average to high flow conditions. For the well-studied Mississippi River, mean daily discharge just above New Orleans for the period 2008–present is 16,120 m<sup>3</sup>/s, with daily ranges from 2,030 m<sup>3</sup>/s to 37,660 m<sup>3</sup>/s. According to Soileau et al. (1990), saltwater penetration occurs over the lower 10s of RKs during low flow periods when discharge is <8,500 m<sup>3</sup>/s, which represents ~18% of all days since 2008. By contrast, discharge values of <4,500 m<sup>3</sup>/s, which has occurred 1.1% of all days since 2008, will allow saltwater wedge intrusion of ~90 RK, and extremely low discharges of <3,350 m<sup>3</sup>/s, which have occurred on 0.2% of all days, will allow saltwater to penetrate upstream ~160 RK.

$B_{ChB}/B_{Ch}$  ratios for the normal flow, upper backwater and lower backwater reaches are summarized in Figure 3 and Table SM10. We find that normal flow reaches have  $B_{ChB}/B_{Ch}$  values that range from ~22 for the highly sinuous Indus River to ~3 for the low sinuosity Niger River, whereas average  $B_{ChB}/B_{Ch}$  values for the lower backwater reach range from 1.78 for the Irrawaddy River to 1.03 for the Indus River, and approach unity ( $B_{ChB}/B_{Ch} \approx 1$ ) in the lowermost reaches of all 5 river systems:  $B_{ChB}/B_{Ch}$  values are, on average, ~8.4 times higher in the normal flow reach relative to the lower backwater reach for all five river systems. We also note that  $B_{ChB}/B_{Ch}$  values display a gradual decrease downstream from  $L_B = 1$ , the estimated location of the normal flow to backwater transition, and through the upper backwater reach in each river system, which extends downstream ~0.6  $L_B$  based on our measurements.

Normal flow  $B_{ChB}/B_{Ch}$  values for the Irrawaddy, Niger and Paraná Rivers overlap with values for the lower backwater reach of the Indus and Mississippi Rivers, which we interpret to indicate that there are no specific uniform scaling relationships for  $B_{ChB}/B_{Ch}$  that apply to all rivers. However, downstream transformations in  $B_{ChB}/B_{Ch}$  between the normal flow and lower backwater reaches within individual river systems are distinct and persistent regardless of river system. Variance in  $B_{ChB}/B_{Ch}$  measurements is also larger in the normal flow reach, ranging from 13.6 for the Indus River to 1.6 for the Niger River, compared to 0.4 to 0.11 for the lower backwater reaches of the Mississippi and Indus rivers, respectively. This variability is interpreted to rep-

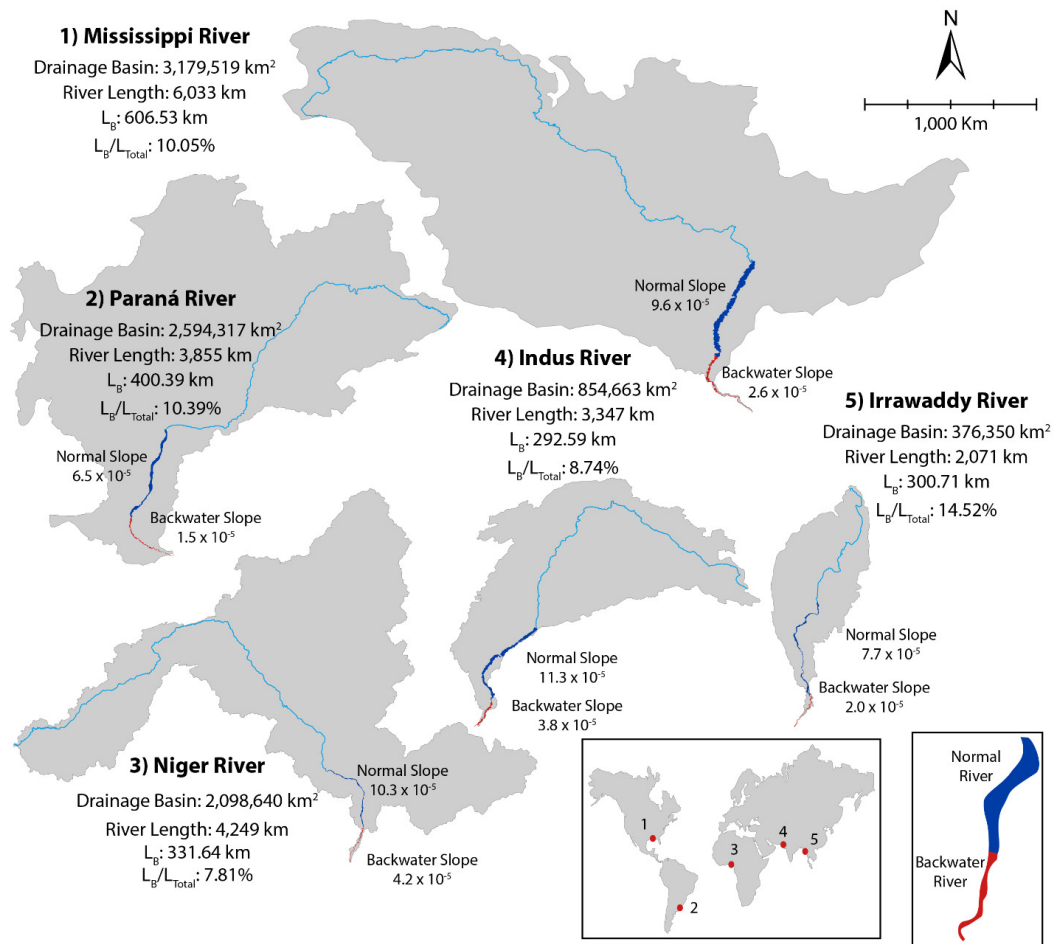


**Figure 2. Comparisons between the five modern rivers in this study. Illustrations highlight drainage basin area (drawn to scale), active primary river channel (light blue), and parts of each river where  $B_{ChB}/B_{Ch}$  and S/M ratios were measured within the normal (dark blue) and backwater (red) reaches for river systems. Gradient measurements are calculated from elevation measurements in Table SM8. Drainage basin and river length data included are from Linke et al. (2019) (Table SM7).**

resent the influence of local bedrock outcrops in limiting lateral migration, and/or the relative maturity of channel curvature since local bedrock may prevent meander loops from increasing their sinuosity, resulting in premature cut-off and abandonment compared to how they would generally mature in a non-bedrock confined part of the system.

Differences in S/M ratios between the normal flow and backwater reaches for each river system correspond to differences in  $B_{ChB}/B_{Ch}$  as well (Figure 3 and Table SM10). Our measurements show that S/M ratios for the normal flow reach range from ~0.83 for the Mississippi River to ~0.50 for the Irrawaddy River, with a mean value of 0.65. By contrast, within the upper backwater reach, S/M ratios decrease to a mean of 0.42, then decrease further in the lower backwater reach to a mean of ~0.07, and approach zero in the lowermost part of each river system. S/M ratio variance in normal flow reaches ranges from 0.3 in the Irrawaddy River to 0.01 in the Mississippi River, with a mean of 0.18, and ranges for lower backwater reach between 0.2 and ~0 for the Mississippi and Indus rivers, respectively, with a mean of 0.14. Both  $B_{ChB}/B_{Ch}$  and S/M ratios therefore illustrate the tendency for greater lateral channel migration and deposi-

tion of sandy channel-belt facies in the normal flow reach, and downstream transformation into significantly reduced  $B_{ChB}/B_{Ch}$  and S/M ratios as each river system goes through the transitional upper, then lower, backwater reaches.

Figure 4a is a cross plot of  $B_{ChB}$  vs.  $B_{Ch}$  to illustrate consistent differences between the normal flow and upper to lower backwater reaches of each river system. As noted above, these metrics overlap for each river system, but  $B_{ChB}$  is, on average, almost an order of magnitude times greater in the normal flow reach relative to the lower backwater reaches for all five rivers we examined. Downstream transformations in  $B_{ChB}$  and  $B_{Ch}$  take place, on average, over the upper 60% of the backwater reach:  $B_{ChB}$  is, on average, only 4.40 and 1.26 times greater than  $B_{Ch}$  in the upper transitional and lower backwater reaches, respectively, clearly indicating downstream decreases in lateral migration (Table SM10). Figure 4b plots probability-density distributions for S/M ratios within the normal flow vs. upper and lower backwater reaches of each river system. These plots show average S/M ratios of 0.65 in the normal flow reach for all five river systems, with values that exceed 0.5 for each river system. Lower S/M ratios characterize the backwater reach

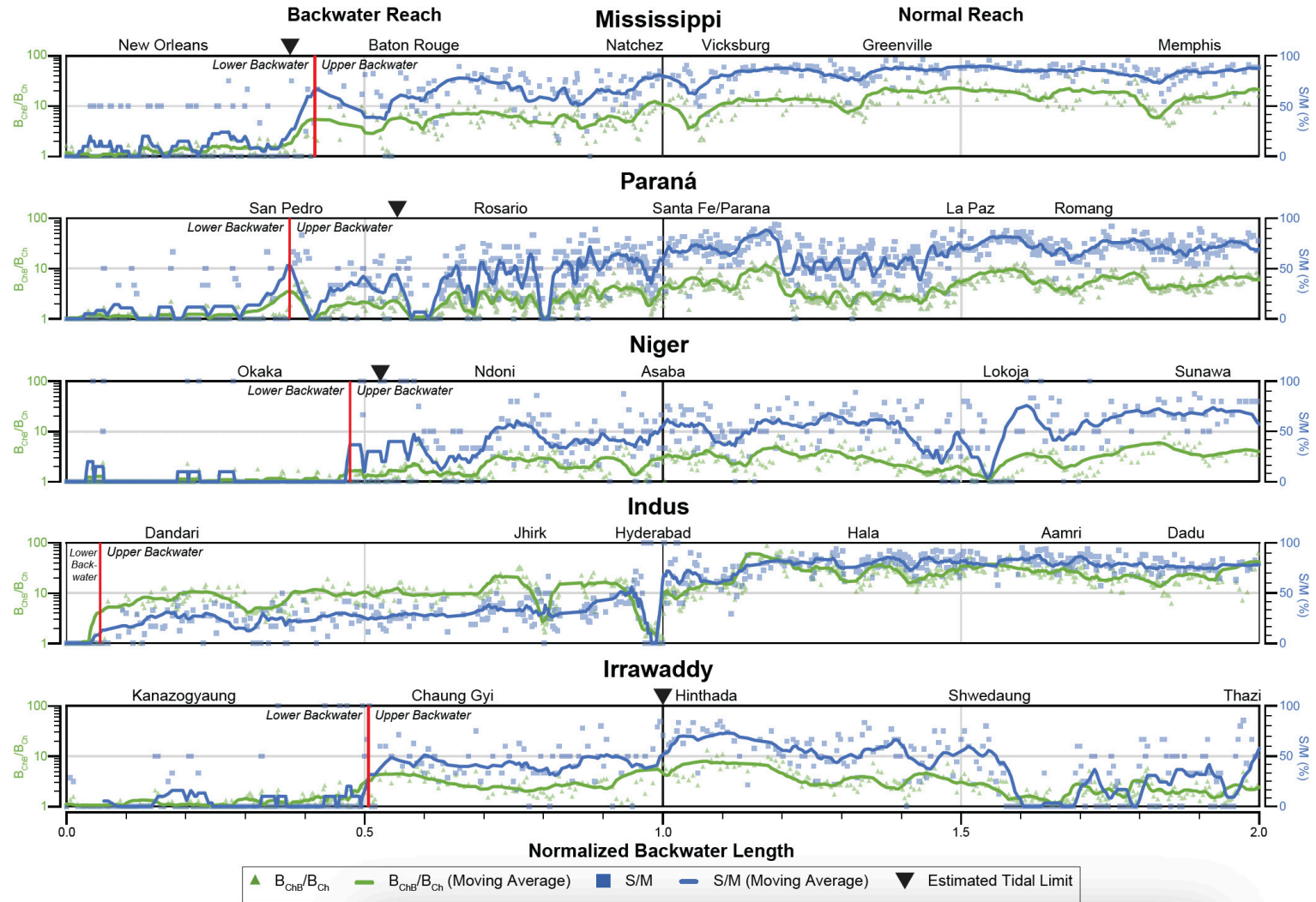


Figure 3.  $B_{ChB}/B_{Ch}$  and S/M ratio plots for the five studied modern rivers. Colored solid lines highlight running averages for data. The x-axis represents the normalized distance from the normal-backwater transition, such that  $L_B = 0$  at river mouth, and each  $L_B$  distance unit represents a backwater length; the first being the backwater reach, and the second is an equivalent distance within the normal reach.



for all river systems, with average values of 0.42 in the upper backwater reach, and 0.07 in the lower backwater reach. As noted above, S/M ratios closely track changes in  $B_{ChB}/B_{Ch}$  and likewise indicate downstream decreasing formation and deposition of laterally accreting sand-rich bar forms.

We considered a number of uncertainties when constructing our dataset. As mentioned, resolution of satellite images is a potential source of uncertainty for our estimates of channel gradients, but there have also been situations where features were too ambiguous to measure (i.e., the exact boundaries of channel belts). We have examined multiple satellite images collected at different times (showing historical maximum migration extent of channel belt) and cited published maps to make or support such interpretations, and suggest that from our calculations, errors in such measurements should not exceed  $\pm 5\%$ . Another area where measurements may show large error is within the S/M ratio dataset since the 500-meter spacing between measurements may, for instance, overestimate the S/M ratio in narrow (<1 km-wide) channel belts (see lower backwater S/M ratio measurements in Figure 3). Other potential areas of error include anthropogenic modifications that impact discharge and sediment loads, and channel migration patterns. Such impacts are especially pertinent to the Mississippi and Indus rivers. Although subject to significant reductions in sediment loads (see Blum & Roberts, 2009; Meade & Moody, 2010; Mize et al., 2018), channel and channel-belt patterns for the Mississippi have essentially been frozen in place by engineering structures, such that our measurements are mostly unaffected. However, in the Indus system, engineering activities resulted in a 70% reduction in water discharge and an 80% reduction in sediment loads following constructions of dams, which in turn led to increases in channel migration rates, and meander wavelengths that are 200–300% larger than they were prior to engineering activities (Syvitski et al., 2014). As a result, our measurements of  $B_{ChB}/B_{Ch}$  and S/M ratios are likely unrepresentative of the Indus River prior to extensive anthropogenic impacts. Regardless, we argue that potential errors in measurement are small and will not change the fundamental insights of this study.

## DISCUSSION AND CONCLUSIONS

Our measurements from modern river systems build on the results of previous workers (e.g., Blum et al., 2013; Fernandes et al., 2016; Martin et al., 2018), and further demonstrate and quantify downstream transformations in morphological and sedimentary characteristics between the normal flow and backwater hydraulic reaches in the five river systems we examined. Our primary findings are consistent with the work of others, and indicate that each river system displays significant reductions in channel gradient, channel migration rates and resultant channel-belt width relative to channel width ( $B_{ChB}/B_{Ch}$ ). Our findings also show gradual decreases in sand-dominated environments and facies, and corresponding increases in mud-dominated environments and facies (S/M ratios) as channels flow through the normal reach to backwater transition

(summarized in Figure 5). We find that the absolute values of  $B_{ChB}/B_{Ch}$  and S/M ratios vary between river systems, and cannot, by themselves, clearly differentiate between the normal flow and backwater reaches within a given system. However, downstream transformations in  $B_{ChB}/B_{Ch}$  and S/M ratios follow the same general trends in all of the systems we have examined. We therefore consider downstream morphological and sedimentary transformations such as these to be inherent to large river systems that discharge to and respond to the presence of the coastal ocean, and they likely pertain to smaller rivers as well (see also Prasojo et al., 2022).

We attribute variation in the absolute values of  $B_{ChB}/B_{Ch}$  and S/M ratios between river systems to bedrock controls on channel migration or, in the case of the Indus River, pervasive anthropogenic modification of discharge, sediment loads, and channel migration rates (Syvitski et al., 2014). Regardless of river system, however, such factors impact morphological and sedimentary characteristics in the normal flow reach more than they do in the backwater reach, as indicated by the higher variance in  $B_{ChB}/B_{Ch}$  and S/M ratio measurements. Channel gradient and lateral channel migration gradually decrease within the upper backwater reach of all 5 river systems, and approach values of 0 within the lower backwater reach, hence variance in measurements becomes correspondingly low. We interpret this trend to indicate the significance of the presence of the coastal ocean as a boundary condition for the parameters we have measured, and to indicate that other factors are less relevant in the lower backwater reach.

The normal flow to backwater hydraulics transition, and the resultant downstream transformations in morphological and sedimentary characteristics represent marine influence. The tidal river is of course also a product of marine influence, and recognition of tidal influences on sedimentary structures within fluvial deposits are traditional indicators of marine influence as well. However, in the 5 systems we studied, the tidal river and the backwater reach are essentially the same only for the macrotidal Irrawaddy River: for the other 4 systems, which have meso- to microtidal regimes at their mouths, the tidal river only extends through 55–62% of the backwater reach. We therefore argue that tide-generated processes have little impact on the 1<sup>st</sup> order downstream morphological and sedimentary transformations that we observe. Instead, they are initiated by changes in hydraulics and sediment transport associated with the normal flow to backwater transition, and would occur in the presence or absence of tides (i.e., in freshwater lake basins or rivers responding to presence of a dam as well). However, tide-generated currents clearly have 2<sup>nd</sup> order effects on the nature of depositional environments and the generation of sedimentary structures within the tidal river, and are known to significantly influence downstream trends in channel width and depth in tide-dominated deltas (see Dalrymple & Choi, 2007; Gugliotta & Saito, 2019).

It is also common to interpret marine influences on the environment of deposition based on recognition criteria that are thought to indicate brackish or saline conditions. However, it is important to place saltwater penetration

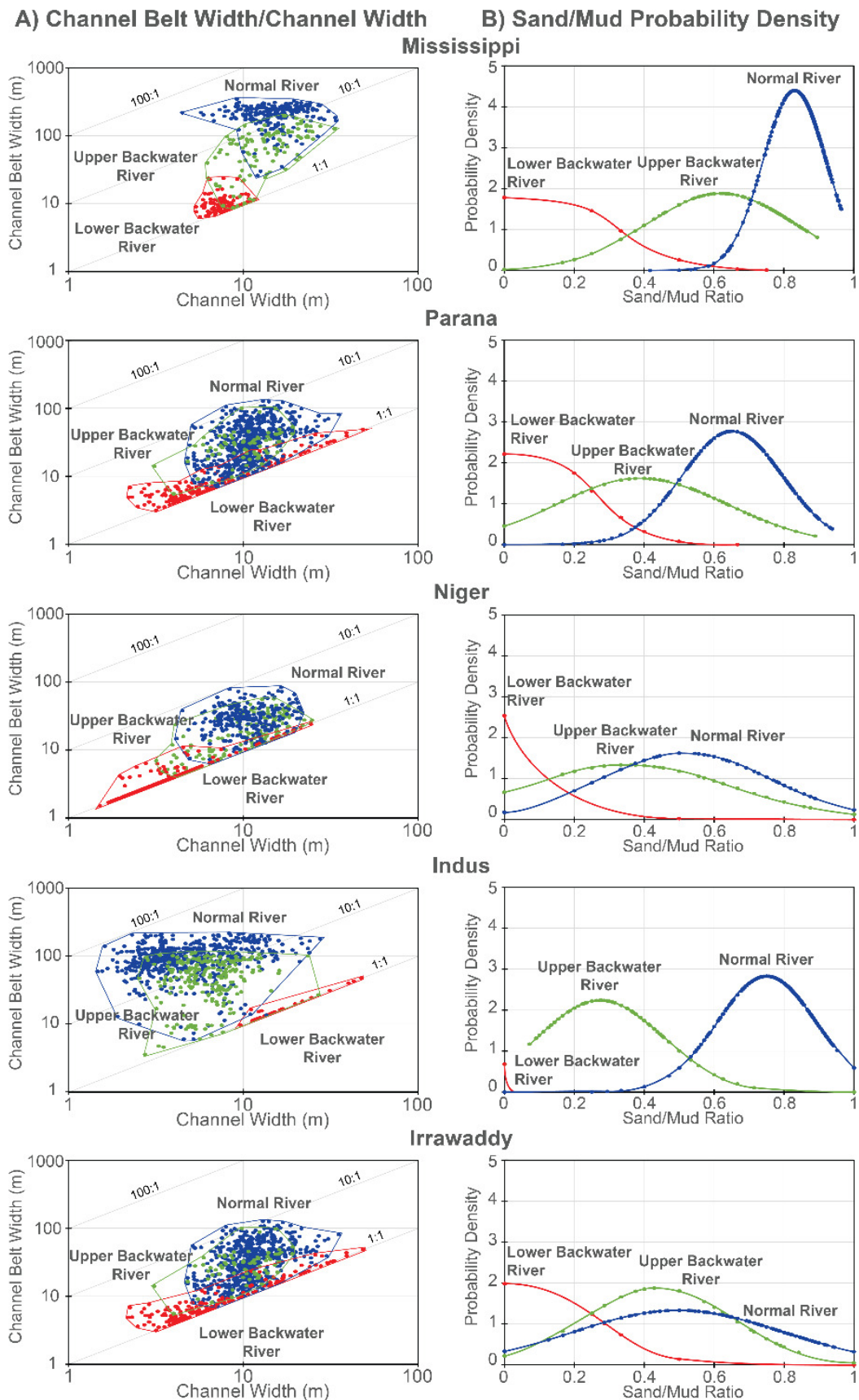


**Figure 4. A) Cross plot of channel-belt width vs. channel width data for the five modern rivers examined. The normal flow parts of each river are plotted in blue, whereas the upper and lower backwater reaches are plotted in green and red, respectively. B) Probability density distribution for S/M ratios in the five modern rivers. As above, normal flow reaches are plotted in blue, whereas upper and lower backwater reaches are plotted in green and red, respectively.**



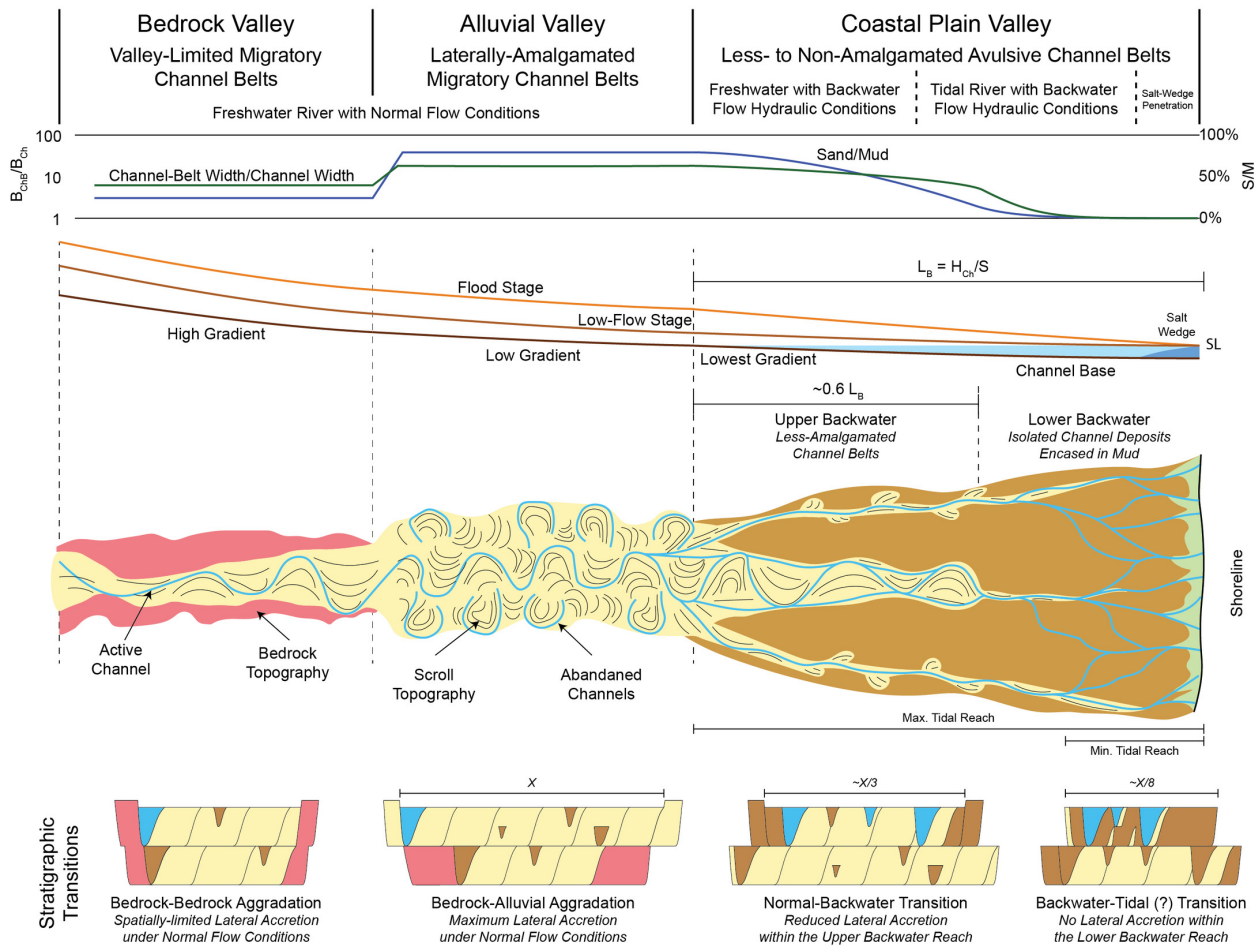


**Figure 5.** A model illustration of changing morphological architecture in response to changing hydraulic conditions in modern river systems. Under normal flow conditions within bedrock and alluvial valleys, changes in channel belt to channel widths ( $B_{ChB}/B_{Ch}$ ) and sand- to mud-dominated (S/M) ratios are attributed to changes in gradient in the more upstream parts of the river system. Under backwater hydraulic conditions in the terminal alluvial to proximal coastal plain valleys, changes in ratios are attributed to the interaction between the river channel water-body and the ensuing marine influence, resulting in a gradually less-sinuuous and less-amalgamated river morphology (reduced  $B_{ChB}/B_{Ch}$  and S/M ratios). Extent of tidal reach is presented based on observations from modern rivers studied. We present model vertical stacking patterns in each segment of our model (drawn to scale) based on measurements in this study. Geomorphic transitions model adapted from Blum (2017).

within the context of scaling relationships. For large river systems, the inland penetration of bottom-hugging saltwater wedges likely has very little impact on the properties of depositional environments, because brackish to saline conditions are uncommon and ephemeral within the upper part of channels above, or upstream from, the saltwater wedge, as well as on the delta plain where freshwater conditions dominate inland from the intertidal zone. Moreover, in large rivers with modest discharge in all seasons, saltwater penetration of more than a few river kilometers is unlikely and may not occur at all. Instead, saltwater wedges only penetrate significant distances (>10 RK) during infrequent seasonal periods of very low discharge, and even then, extreme saltwater wedge penetration (>100 RK) only occurs over ~50% of the length of the tidal river. Hence, marine saltwater penetration is limited to the lower half of the tidal river, saltwater penetration does not extend into

the normal flow or upper backwater reaches, and saltwater penetration distances do not overlap with high values of  $B_{ChB}/B_{Ch}$  and S/M ratios that characterize the normal flow and upper backwater reaches.

We conclude that quantification of dimensionless scaling relationships in modern environments can provide an empirical framework for how morphological and sedimentary patterns form over time and space. For example, sand body geometries and the spatial distribution of sand-rich vs. mud-dominated fluvial facies can, in general, be predicted and modeled at the 1<sup>st</sup> order within different segments of river systems when contextualized as scaling relationships (e.g.,  $B_{ChB}/B_{Ch}$  and S/M ratios) that are derived from modern river systems, rather than focusing on the actual dimensions themselves. Empirically-defined scaling relationships can also be applied to the stratigraphic record, such that dimensionless relationships measured in

more proximal to more distal settings within ancient strata can be used to constrain the hydraulic context and paleogeographic position for ancient fluvial-deltaic successions (Figure 5).

.....

## Acknowledgments

The authors would like to acknowledge the Scott and Carol Ritchie professorship at the University of Kansas. we also would like to thank the editor Dr. Jeong-Hyun Lee, and all reviewers, including Dr. Chris Paola and Dr. Bjorn Nyberg.

Submitted: March 05, 2023 CST, Accepted: November 10, 2023 CST



This is an open-access article distributed under the terms of the Creative Commons Attribution 4.0 International License (CCBY-4.0). View this license's legal deed at <http://creativecommons.org/licenses/by/4.0> and legal code at <http://creativecommons.org/licenses/by/4.0/legalcode> for more information.

## References

- Abam, T. K. S., & Fubara, D. M. J. (2022). Analysis of Hydrological Characteristics: A Case Review of the Niger Delta. *Journal of Water Resource and Protection*, 14(9), 611–631. <https://doi.org/10.4236/jwarp.2022.149032>
- Abam, T. K. S., & Omuso, W. O. (2000). On river cross-sectional change in the Niger Delta. *Geomorphology*, 34(1–2), 111–126. [https://doi.org/10.1016/s0169-555x\(99\)00129-4](https://doi.org/10.1016/s0169-555x(99)00129-4)
- Allen, P. A. (2008). From landscapes into geological history. *Nature*, 451(7176), 274–276. <https://doi.org/10.1038/nature06586>
- Blum, M. D. (2017). The McMurray conundrum. *Reservoir*, 2, 25–29.
- Blum, M. D., Martin, J., Milliken, K., & Garvin, M. (2013). Paleovalley systems: insights from Quaternary analogs and experiments. *Earth-Science Reviews*, 116, 128–169. <https://doi.org/10.1016/j.earscirev.2012.09.003>
- Blum, M. D., Milliken, K. T., Pecha, M. A., Snedden, J. W., Frederick, B. C., & Galloway, W. E. (2017). Detrital-zircon records of Cenomanian, Paleocene, and Oligocene Gulf of Mexico drainage integration and sediment routing: Implications for scales of basin-floor fans. *Geosphere*, 13(6), 2169–2205. <http://doi.org/10.1130/ges01410.1>
- Blum, M. D., & Roberts, H. H. (2009). Drowning of the Mississippi Delta due to insufficient sediment supply and global sea-level rise. *Nature Geoscience*, 2(7), 488–491. <https://doi.org/10.1038/ngeo553>
- Brice, J. C. (1974). Evolution of meander loops. *Geological Society of America Bulletin*, 85(4), 581–586. [https://doi.org/10.1130/0016-7606\(1974\)85](https://doi.org/10.1130/0016-7606(1974)85)
- Carey, W. C. (1969). Formation of flood plain lands. *Journal of the Hydraulics Division*, 95(3), 981–994. <http://doi.org/10.1061/jyceaj.0002112>
- Carlin, J. A., Dellapenna, T. M., Strom, K., & Noll, C. J., IV. (2015). The influence of a salt wedge intrusion on fluvial suspended sediment and the implications for sediment transport to the adjacent coastal ocean: a study of the lower Brazos River TX, USA. *Marine Geology*, 359, 134–147. <https://doi.org/10.1016/j.margeo.2014.11.001>
- Chamberlin, E. P., & Hajek, E. A. (2019). Using bar preservation to constrain reworking in channel-dominated fluvial stratigraphy. *Geology*, 47(6), 531–534. <https://doi.org/10.1130/g46046.1>
- Church, M. (2006). Bed material transport and the morphology of alluvial river channels. *Annual Review of Earth and Planetary Sciences*, 34(1), 325–354. <http://doi.org/10.1146/annurev.earth.33.092203.122721>
- Dade, W. B. (2000). Grain size, sediment transport and alluvial channel pattern. *Geomorphology*, 35(1–2), 119–126. [https://doi.org/10.1016/s0169-555x\(00\)00030-1](https://doi.org/10.1016/s0169-555x(00)00030-1)
- Dade, W. B., & Friend, P. F. (1998). Grain-size, sediment-transport regime, and channel slope in alluvial rivers. *The Journal of Geology*, 106(6), 661–676. <https://doi.org/10.1086/516052>
- Dalrymple, R. W., & Choi, K. (2007). Morphologic and facies trends through the fluvial–marine transition in tide-dominated depositional systems: a schematic framework for environmental and sequence-stratigraphic interpretation. *Earth-Science Reviews*, 81(3–4), 135–174. <https://doi.org/10.1016/j.earscirev.2006.10.002>
- Densmore, A. L., Allen, P. A., & Simpson, G. (2007). Development and response of a coupled catchment fan system under changing tectonic and climatic forcing. *Journal of Geophysical Research: Earth Surface*, 112(F1). <https://doi.org/10.1029/2006jf000474>
- Eisma, D. (1998). *Intertidal Deposits: River mouths, Tidal Flats and Coastal Lagoons*. CRC Press.
- Fernandes, A. M., Törnqvist, T. E., Straub, K. M., & Mohrig, D. (2016). Connecting the backwater hydraulics of coastal rivers to fluvio-deltaic sedimentology and stratigraphy. *Geology*, 44(12), 979–982. <https://doi.org/10.1130/g37965.1>
- Flint, J. J. (1974). Stream gradient as a function of order, magnitude, and discharge. *Water Resources Research*, 10(5), 969–973. <https://doi.org/10.1029/wr010i005p00969>
- Galler, J. J., & Allison, M. A. (2008). Estuarine controls on fine-grained sediment storage in the Lower Mississippi and Atchafalaya Rivers. *Geological Society of America Bulletin*, 120(3–4), 386–398. <https://doi.org/10.1130/b26060.1>
- Ganti, V., Hassenruck-Gudipati, H. J., Chadwick, A. J., & Lamb, M. P. (2014). *Mechanics of Backwater-Mediated Avulsions on River Deltas*. The AGU Fall Meeting Abstracts.
- Geyer, W. R., & MacCready, P. (2014). The estuarine circulation. *Annual Review of Fluid Mechanics*, 46(1), 175–197. <https://doi.org/10.1146/annurev-fluid-010313-141302>
- Gingras, M. K., & Leckie, D. A. (2017). The argument for tidal and brackish water influence in the McMurray Formation reservoirs. *Reservoir*, 2, 21–24.
- Giosan, L., Constantinescu, S., Clift, P. D., Tabrez, A. R., Danish, M., & Inam, A. (2006). Recent morphodynamics of the Indus delta shore and shelf. *Continental Shelf Research*, 26(14), 1668–1684. <http://doi.org/10.1016/j.csr.2006.05.009>
- Gugliotta, M., & Saito, Y. (2019). Matching trends in channel width, sinuosity, and depth along the fluvial to marine transition zone of tide-dominated river deltas: the need for a revision of depositional and hydraulic models. *Earth-Science Reviews*, 191, 93–113. <https://doi.org/10.1016/j.earscirev.2019.02.002>
- Harleman, D. R. F. (1991). Keulegan legacy. Saline wedges. *Journal of Hydraulic Engineering*, 117(12), 1616–1625. [https://doi.org/10.1061/\(asce\)0733-9429\(1991\)117:12\(1616\)](https://doi.org/10.1061/(asce)0733-9429(1991)117:12(1616))



- Hartley, A. J., Weissmann, G. S., & Scuderi, L. (2017). Controls on the apex location of large deltas. *Journal of the Geological Society*, 174(1), 10–13. <https://doi.org/10.1144/jgs2015-154>
- Hedley, P. J., Bird, M. I., & Robinson, R. A. J. (2010). Evolution of the Irrawaddy delta region since 1850. *Geographical Journal*, 176(2), 138–149. <https://doi.org/10.1111/j.1475-4959.2009.00346.x>
- Hickin, E. J. (1974). The development of meanders in natural river-channels. *American Journal of Science*, 274(4), 414–442. <https://doi.org/10.2475/ajs.274.4.414>
- Hickin, E. J., & Nanson, G. C. (1975). The character of channel migration on the Beatton River, northeast British Columbia, Canada. *Geological Society of America Bulletin*, 86(4), 487–494. [https://doi.org/10.1130/0016-7606\(1975\)86](https://doi.org/10.1130/0016-7606(1975)86)
- Hudson, P. F., & Kesel, R. H. (2000). Channel migration and meander-bend curvature in the lower Mississippi River prior to major human modification. *Geology*, 28(6), 531–534. [https://doi.org/10.1130/0091-7613\(2000\)28](https://doi.org/10.1130/0091-7613(2000)28)
- Ibañez, C., Pont, D., & Prat, N. (1997). Characterization of the Ebre and Rhone estuaries: A basis for defining and classifying salt-wedge estuaries. *Limnology and Oceanography*, 42(1), 89–101. <https://doi.org/10.4319/lo.1997.42.1.0089>
- Jackson, R. G. (1976). Depositional model of point bars in the lower Wabash River. *Journal of Sedimentary Research*, 46(3), 579–594.
- Jerolmack, D. J., & Swenson, J. B. (2007). Scaling relationships and evolution of distributary networks on wave-influenced deltas. *Geophysical Research Letters*, 34(23). <https://doi.org/10.1029/2007gl031823>
- Jobe, Z. R., Howes, N. C., Straub, K. M., Cai, D., Deng, H., Laugier, F. J., Pettinga, L. A., & Shumaker, L. E. (2020). Comparing aggradation, superelevation, and avulsion frequency of submarine and fluvial channels. *Frontiers in Earth Science*, 8, 53. <https://doi.org/10.3389/feart.2020.00053>
- Kineke, G. C., & Sternberg, R. W. (1995). Distribution of fluid muds on the Amazon continental shelf. *Marine Geology*, 125(3–4), 193–233. [https://doi.org/10.1016/0025-3227\(95\)00013-0](https://doi.org/10.1016/0025-3227(95)00013-0)
- Knighton, D. (1992). *Fluvial Forms and Processes*. Edward Arnold Ltd.
- Kravtsova, V. I., Mikhailov, V. N., & Kozyukhina, A. S. (2008). Hydrological-morphological and landscape features of the Niger River delta. *Water Resources*, 35(2), 121–136. <https://doi.org/10.1134/s0097807808020012>
- Langbein, W. B. (1964). Geometry of river channels. *Journal of the Hydraulics Division*, 90(2), 301–312. <https://doi.org/10.1061/jycej.0001019>
- Langbein, W. B., & Leopold, L. B. (1970). *River meanders and the theory of minimum variance Rivers and river terraces*. Springer.
- Leopold, L. B., & Langbein, W. B. (1966). River meanders. *Scientific American*, 214(6), 60–73. <https://doi.org/10.1038/scientificamerican0666-60>
- Leopold, L. B., & Maddock, T. (1953). *The hydraulic geometry of stream channels and some physiographic implications* (Vol. 252). US Government Printing Office.
- Leopold, L. B., & Wolman, M. G. (1960). River meanders. *Geological Society of America Bulletin*, 71(6), 769–793. [https://doi.org/10.1130/0016-7606\(1960\)71](https://doi.org/10.1130/0016-7606(1960)71)
- Leuven, J. R. F. W., van Maanen, B., Lexmond, B. R., van der Hoek, B. V., Spruijt, M. J., & Kleinans, M. G. (2018). Dimensions of fluvial-tidal meanders: Are they disproportionally large? *Geology*, 46(10), 923–926. <https://doi.org/10.1130/g45144.1>
- Lewin, J. (1983). *Changes of channel patterns and floodplains*. The Background to palaeohydrology. A perspective.
- Li, C., Wang, P., Fan, D., & Yang, S. (2006). Characteristics and formation of Late Quaternary incised-valley-fill sequences in sediment-rich deltas and estuaries: case studies from China. *SEPM Special Publication*, 85.
- Linke, S., Lehner, B., Ouellet, D. C., Ariwi, J., Grill, G., Anand, M., Beames, P., Burchard-Levine, V., Maxwell, S., Moidu, H., Tan, F., & Thieme, M. (2019). Global hydro-environmental sub-basin and river reach characteristics at high spatial resolution. *Scientific Data*, 6(1), 1–15. <https://doi.org/10.1038/s41597-019-0300-6>
- Martin, J., Fernandes, A. M., Pickering, J., Howes, N., Mann, S., & McNeil, K. (2018). The stratigraphically preserved signature of persistent backwater dynamics in a large paleodelta system: The Mungaroo Formation, North West Shelf, Australia. *Journal of Sedimentary Research*, 88(7), 850–872. <https://doi.org/10.2110/jsr.2018.38>
- Matsoukis, C., Amoudry, L. O., Bricheno, L., & Leonardi, N. (2023). Numerical investigation of river discharge and tidal variation impact on salinity intrusion in a generic river delta through idealized modelling. *Estuaries and Coasts*, 46(1), 57–83. <https://doi.org/10.1007/s12237-022-01109-2>
- Meade, R. H., & Moody, J. A. (2010). Causes for the decline of suspended-sediment discharge in the Mississippi River system, 1940–2007. *Hydrological Processes: An International Journal*, 24(1), 35–49.
- Milliken, K. T., Blum, M. D., Snedden, J. W., & Galloway, W. E. (2018). Application of fluvial scaling relationships to reconstruct drainage-basin evolution and sediment routing for the Cretaceous and Paleocene of the Gulf of Mexico. *Geosphere*, 14(2), 749–767. <https://doi.org/10.1130/ges01374.1>
- Milliman, J. D., & Farnsworth, K. L. (2013). *River discharge to the coastal ocean: a global synthesis*. Cambridge University Press.
- Mize, S. V., Murphy, J. C., Diehl, T. H., & Demcheck, D. K. (2018). Suspended-sediment concentrations and loads in the lower Mississippi and Atchafalaya rivers decreased by half between 1980 and 2015. *Journal of Hydrology*, 564, 1–11. <https://doi.org/10.1016/j.jhydro.2018.05.068>

- Moreton, D. J., & Carter, B. J. (2015). Characterizing alluvial architecture of point bars within the McMurray Formation, Alberta, Canada, for improved bitumen resource prediction and recovery. *Developments in Sedimentology*, 68, 529–559.
- Nittrouer, J. A., Shaw, J., Lamb, M. P., & Mohrig, D. (2011). Spatial and temporal trends for water-flow velocity and bed-material sediment transport in the lower Mississippi River. *Geological Society of America Bulletin*, 124(3–4), 400–414. <https://doi.org/10.1130/b30497.1>
- Nyberg, B., Gawthorpe, R. L., & Helland-Hansen, W. (2018). The distribution of rivers to terrestrial sinks: implications for sediment routing systems. *Geomorphology*, 316, 1–23. <https://doi.org/10.1016/j.geomorph.2018.05.007>
- Nyberg, B., Helland-Hansen, W., Gawthorpe, R. L., Sandbakken, P., Eide, C. H., Sømme, T., Hadler-Jacobsen, F., & Leiknes, S. (2018). Revisiting morphological relationships of modern source-to-sink segments as a first-order approach to scale ancient sedimentary systems. *Sedimentary Geology*, 373, 111–133. <https://doi.org/10.1016/j.sedgeo.2018.06.007>
- Nyberg, B., Henstra, G., Gawthorpe, R. L., Ravnås, R., & Ahokas, J. (2023). Global scale analysis on the extent of river channel belts. *Nature Communications*, 14(1), 2163. <https://doi.org/10.1038/s41467-023-37852-8>
- Obowu, C. D., & Abam, T. K. S. (2014). Spatial and multi-temporal change analysis of the Niger Delta coastline using remote sensing and geographic information system (GIS). *International Journal of Remote Sensing Applications*, 4(1), 41. <https://doi.org/10.14355/ijrsa.2014.0401.04>
- Paola, C., & Martin, J. M. (2012). Mass-balance effects in depositional systems. *Journal of Sedimentary Research*, 82(6), 435–450. <https://doi.org/10.2110/jsr.2012.38>
- Paola, C., & Mohrig, D. (1996). Palaeohydraulics revisited: Palaeoslope estimation in coarse-grained braided rivers. *Basin Research*, 8(3), 243–254. <https://doi.org/10.1046/j.1365-2117.1996.00253.x>
- Parsa, J., & Shahidi, A. E. (2010). Prediction of tidal excursion length in estuaries due to the environmental changes. *International Journal of Environmental Science & Technology*, 7(4), 675–686. <https://doi.org/10.1007/bf03326177>
- Passalacqua, P., Lanzoni, S., Paola, C., & Rinaldo, A. (2013). Geomorphic signatures of deltaic processes and vegetation: The Ganges-Brahmaputra-Jamuna case study. *Journal of Geophysical Research: Earth Surface*, 118(3), 1838–1849.
- Peng, Y., Hagstrom, C. A., Horner, S. C., Hodgson, C. A., Martin, H. K., Leckie, D. A., Pedersen, P. K., & Hubbard, S. M. (2022). Low-accommodation foreland basin response to long-term transgression: A record of change from continental-fluvial and marginal-marine to open-marine sequences over 60,000 km<sup>2</sup> in the western Canada foreland basin. *Marine and Petroleum Geology*, 139, 105583. <https://doi.org/10.1016/j.marpetgeo.2022.105583>
- Prasojo, O. A., Hoey, T. B., Owen, A., & Williams, R. D. (2022). Slope break and avulsion locations scale consistently in global deltas. *Geophysical Research Letters*, 49(2), 2021093656. <https://doi.org/10.1029/2021gl093656>
- Prokocki, E. W. (2017). *The sedimentology of bedforms to barforms within tidally-influenced fluvial zones (TIFZx): lower Columbia River, OR/WA, USA, and the lower Chehalis River, WA, USA* [PhD]. University of Illinois at Urbana-Champaign.
- Romans, B. W., Castelltort, S., Covault, J. A., Fildani, A., & Walsh, J. P. (2016). Environmental signal propagation in sedimentary systems across timescales. *Earth-Science Reviews*, 153, 7–29. <https://doi.org/10.1016/j.earscirev.2015.07.012>
- Sakai, T., Omori, K., Oo, A. N., & Zaw, Y. N. (2021). Monitoring saline intrusion in the Ayeyarwady Delta, Myanmar, using data from the Sentinel-2 satellite mission. *Paddy and Water Environment*, 19, 283–294. <https://doi.org/10.1007/s10333-020-00837-0>
- Sandbach, S. D., Nicholas, A. P., Ashworth, P. J., Best, J. L., Keevil, C. E., Parsons, D. R., Prokocki, E. W., & Simpson, C. J. (2018). Hydrodynamic modelling of tidal-fluvial flows in a large river estuary. *Estuarine, Coastal and Shelf Science*, 212, 176–188. <https://doi.org/10.1016/j.ecss.2018.06.023>
- Schumm, S. A. (1977). *The fluvial system*.
- Shchepetkina, A., Gingras, M. K., Mángano, M. G., & Buatois, L. A. (2019). Fluvio-tidal transition zone: Terminology, sedimentological and ichnological characteristics, and significance. *Earth-Science Reviews*, 192, 214–235. <https://doi.org/10.1016/j.earscirev.2019.03.001>
- Shchepetkina, A., Gingras, M. K., Pemberton, S. G., MacEachern, J. A., & Plint, G. (2016). What does the ichnological content of the Middle McMurray Formation tell us? *Bulletin of Canadian Petroleum Geology*, 64(1), 24–46. <https://doi.org/10.2113/gscpgbull.64.1.24>
- Sincavage, R. S., Paola, C., & Goodbred, S. L., Jr. (2019). Coupling mass extraction and downstream fining with fluvial facies changes across the Sylhet basin of the Ganges-Brahmaputra-Meghna Delta. *Journal of Geophysical Research: Earth Surface*, 124(2), 400–413. <https://doi.org/10.1029/2018jf004840>
- Soileau, C. W., Garrett, B. J., Thibodeaux, B. J., & Magoon, O. T. (1990). Drought induced saltwater intrusion on the Mississippi River. *Coastal & Inland Water Quality*, 223–234.
- Sømme, T. O., Helland-Hansen, W., Martinsen, O. J., & Thurmond, J. B. (2009). Relationships between morphological and sedimentological parameters in source-to-sink systems: a basis for predicting semi-quantitative characteristics in subsurface systems. *Basin Research*, 21(4), 361–387. <https://doi.org/10.1111/j.1365-2117.2009.00397.x>
- Strong, N., Sheets, B., Hickson, T., & Paola, C. (2005). A mass-balance framework for quantifying downstream changes in fluvial architecture. *Fluvial Sedimentology*, VII, 243–253. <https://doi.org/10.1002/9781444304350.ch14>

- Syvitski, J. P. M., Anthony, E., Saito, Y., Zăinescu, F., Day, J., Bhattacharya, J. P., & Giosan, L. (2022). Large deltas, small deltas: toward a more rigorous understanding of coastal marine deltas. *Global and Planetary Change*, 218, 103958. <https://doi.org/10.1016/j.gloplacha.2022.103958>
- Syvitski, J. P. M., Kettner, A. J., Overeem, I., Giosan, L., Brakenridge, G. R., Hannon, M., & Bilham, R. (2014). Anthropocene metamorphosis of the Indus Delta and lower floodplain. *Anthropocene*, 3, 24–35. <https://doi.org/10.1016/j.ancene.2014.02.003>
- Syvitski, J. P. M., & Milliman, J. D. (2007). Geology, geography, and humans battle for dominance over the delivery of fluvial sediment to the coastal ocean. *The Journal of Geology*, 115(1), 1–19. <https://doi.org/10.1086/509246>
- Taft, L., & Evers, M. (2016). A review of current and possible future human–water dynamics in Myanmar’s river basins. *Hydrology and Earth System Sciences*, 20(12), 4913–4928. <https://doi.org/10.5194/hess-20-4913-2016>
- Velden, J. (2015). *Understanding river dynamics of the Ayeyarwady River, Myanmar How dynamic behaviour contributes to adapting the river morphology for navigational purposes* [MS Thesis]. Utrecht University.
- Wahbi, A. M., Blum, M. D., & Nazworth Doerger, C. (2022). Early Cretaceous continental-scale sediment routing, the McMurray Formation, Western Canada Sedimentary Basin, Alberta, Canada. *GSA Bulletin*, 135(7–8), 2088–2106. <https://doi.org/10.1130/b36412.1>
- Wang, J., Li, L., He, Z., Kalhor, N. A., & Xu, D. (2019). Numerical modelling study of seawater intrusion in Indus River Estuary, Pakistan. *Ocean Engineering*, 184, 74–84. <https://doi.org/10.1016/j.oceaneng.2019.05.029>
- Wilson, C. A., & Goodbred, S. L., Jr. (2015). Construction and maintenance of the Ganges-Brahmaputra-Meghna delta: linking process, morphology, and stratigraphy. *Annual Review of Marine Science*, 7(1), 67–88. <https://doi.org/10.1146/annurev-marine-010213-135032>



## Supplementary Materials

### Supplementary Material Key

Download: <https://thesedimentaryrecord.scholasticahq.com/article/90009-downstream-morphological-and-sedimentary-transformations-in-modern-continental-scale-rivers/attachment/186556.pdf>

---

### Table SM1

Download: <https://thesedimentaryrecord.scholasticahq.com/article/90009-downstream-morphological-and-sedimentary-transformations-in-modern-continental-scale-rivers/attachment/186558.xlsx>

---

### Table SM2

Download: <https://thesedimentaryrecord.scholasticahq.com/article/90009-downstream-morphological-and-sedimentary-transformations-in-modern-continental-scale-rivers/attachment/186557.xlsx>

---

### Table SM3

Download: <https://thesedimentaryrecord.scholasticahq.com/article/90009-downstream-morphological-and-sedimentary-transformations-in-modern-continental-scale-rivers/attachment/186555.xlsx>

---

### Table SM4

Download: <https://thesedimentaryrecord.scholasticahq.com/article/90009-downstream-morphological-and-sedimentary-transformations-in-modern-continental-scale-rivers/attachment/186553.xlsx>

---

### Table SM5

Download: <https://thesedimentaryrecord.scholasticahq.com/article/90009-downstream-morphological-and-sedimentary-transformations-in-modern-continental-scale-rivers/attachment/186550.xlsx>

---

### Table SM6

Download: <https://thesedimentaryrecord.scholasticahq.com/article/90009-downstream-morphological-and-sedimentary-transformations-in-modern-continental-scale-rivers/attachment/186552.xlsx>

---

### Table SM7

Download: <https://thesedimentaryrecord.scholasticahq.com/article/90009-downstream-morphological-and-sedimentary-transformations-in-modern-continental-scale-rivers/attachment/186554.xlsx>

---

### Table SM8

Download: <https://thesedimentaryrecord.scholasticahq.com/article/90009-downstream-morphological-and-sedimentary-transformations-in-modern-continental-scale-rivers/attachment/186551.xlsx>

---

### Table SM9

---

Download: <https://thesedimentaryrecord.scholasticahq.com/article/90009-downstream-morphological-and-sedimentary-transformations-in-modern-continental-scale-rivers/attachment/186549.xlsx>

---

## Table SM10

Download: <https://thesedimentaryrecord.scholasticahq.com/article/90009-downstream-morphological-and-sedimentary-transformations-in-modern-continental-scale-rivers/attachment/186548.xlsx>

---